Case Studies in Thermal Engineering 45 (2023) 102973

Contents lists available at ScienceDirect

Case Studies in Thermal Engineering

journal homepage: www.elsevier.com/locate/csite

Influence of uniform magnetic field on hydrothermal characteristics and entropy production in a nanofluid filled rectangular grooved channel

Sergen Tumse [a], Besir Sahin [a,b,*]

[a] Cukurova University, Faculty of Engineering, Mechanical Engineering Department, Adana 01330, Turkiye
[b] Istanbul Aydin University, Faculty of Engineering, Aerospace Engineering Department, Istanbul, 34295, Turkiye

ARTICLE INFO

Handling EditorHuihe Qiu

Keywords:
Magnetohydrodynamic
Magnetic field
Rectangular grooved channel
Heat transfer
Forced convection
Flow control
Entropy generation
Nusselt number

ABSTRACT

The implementation of a uniform magnetic field can be beneficial for controlling thermal convective processes in magneto-thermal devices and systems. In research of productive energy employment and superior thermal efficiency, the present numerical research study aimed to investigate the flow structure, thermal behaviors, and entropy production of nanofluids with a mixture of CuO and water in a rectangular grooved channel subjected to the uniform magnetic field in the transverse direction. Convective dynamics in such rectangular grooved channels subjected to a uniform magnetic field have not been comprehensively investigated considering flow structures, thermal performances and entropy characteristics. The impact of different variables namely nanoparticle volume concentrations, Φ Hartmann numbers, Ha and Reynolds numbers, Re on the hydrothermal characteristics is numerically explored. According to acquired outcomes, the uniformly implemented magnetic field in the rectangular grooved channel causes significant variations of flow characteristics demonstrated by the streamline patterns and reduces the extent of the recirculation flow zone in rectangular grooves at $Re = 250$ and 1250. During the application of the uniform magnetic field, the thermal boundary layer formed in the rectangular grooves becomes thinner, while the temperature gradient in the near regions of the heated walls increases. Numerical simulations show that the average Nusselt number, Nu_{avg} increases by approximately 9.08% for $Ha = 8$ and 30.42% for $Ha = 24$ at $Re = 250$, and by 0.087% for $Ha = 8$ and 21.13% for $Ha = 24$ at $Re = 1250$, compared to the case where no uniform magnetic field is applied, $Ha = 0$. It can be observed that for a given value of Re, the total entropy reduces sharply for $Ha > 8$, due to the significant effect of high magnetic field intensity over both thermal and flow distributions. The outputs of this study could be very beneficial for designers modeling any device or system including thermal energy transportation in various industrial applications such as cooling circuits of electronic components and fast fission reactors, materials science and metallurgical processes.

* Corresponding author. Istanbul Aydin University, Faculty of Engineering, Aerospace Engineering Department, Istanbul, 34295, Turkiye.
E-mail addresses: besirsahin@aydin.edu.tr, bsahin@cu.edu.tr (B. Sahin).

https://doi.org/10.1016/j.csite.2023.102973
Received 7 January 2023; Received in revised form 13 March 2023; Accepted 31 March 2023
Available online 5 April 2023

Nomenclature

B_0	applied magnetic field (Tesla)
Be	Bejan number
C_p	specific heat (J/kg.K)
Cr	Courant number
f	friction factor
g	gravitational acceleration (m/s^2)
H	channel height (m)
Ha	Hartmann number
k	thermal conductivity, (W/m.K)
l	groove length (m)
Lg	length of a grooved section (m)
Ls	length of the straight section (m)
Lw	length of the rectangular corrugated wall (m)
Nu	Nusselt number
NuL	local Nusselt number
$\overline{p}$	pressure (Pa)
p	dimensionless pressure
Pr	Prandtl number
Ra	Rayleigh number
Re	Reynolds number
$\overline{s}_L$	dimensional total entropy generation, (W/K.m^3)
s_L	non-dimensional total entropy generation
$\overline{t}$	time (s)
t	non-dimensional time
T	temperature (K)
T_o	average temperature (K)
$\overline{u}, \overline{v}$	velocity components in $\overline{x}$ and $\overline{y}$ directions, respectively (m/s)
u, v	dimensionless velocity components
$\overline{x}, \overline{y}$	dimensional Cartesian coordinates (m)
x, y	non-dimensional Cartesian coordinates
χ	irreversible factor

Greek letters

α	thermal diffusivity (m^2/s)
β	thermal expansion coefficient (1/K)
θ	non-dimensional temperature
μ	dynamic viscosity (Pa.s)
ν	kinematic viscosity (m^2/s)
ρ	density (kg/m^3)
σ	electrical conductivity (S/m)
Φ	volume fraction of nanoparticles
¥	magnetic field inclination angle

Subscripts

nf	nanofluid
bf	base fluid
np	nanoparticles
h	hot
c	cold
avg	average
th	thermal
vis	viscous
mag	magnetic
i	inlet

1. Introduction

Nowadays, energy transfer, particularly heat transfer is a significant concern in various fields such as industry, engineering, manufacturing and transportation. The energy efficiency perspective demands compact heat exchangers and air conditioning systems with high heat transfer efficiency. The performance of the heat exchanger requires to be substantially enhanced by employing heat transfer improvement methods to obtain both great heat transfer efficiency and compact designs opportunity.

The heat transfer augmentation techniques in various types of energy systems with the goal of achieving optimal design and efficiency, are composed of active, passive, and compound flow control techniques. The application of grooved and ribbed surfaces as a passive heat transfer augmentation technique is prevalent in engineering and industrial fields [1]. In the investigation of Tokgoz et al. [2], it was found that thermal boundary layers along rectangular grooved channel get thinner compared to straight channel flow having no corrugations and the occurrence of vorticities in the rectangular grooves enhances heat transfer performance. The use of a rectangular grooved channel leads to an increase in pressure loss, even as average Nusselt number, Nu_{avg} increases [3]. According to Hamzah et al. [4], utilizing SWCNT-water nanofluid in a sinusoidally corrugated channel is an impressive technique to augment heat transfer efficiency and diminish thermal irreversibility. The heat transfer augmentation in sinusoidally corrugated channel is not important at lower amplitude wavelength ratios, but at an adequately higher amplitude wavelength ratios, the sinusoidally corrugated channel is observed to be influential heat transfer geometry particularly at greater *Re* [5]. Aly et al. [6] carried out the ISPH (incompressible smoothed particle hydrodynamic) method to investigate the mixed convection in an inclined lid-driven cavity with sinusoidal heated walls. They stated that the shear force caused by lid-movement demonstrates a more dominant effect than the inclination angle of the cavity. For further studies on the hydrothermal behaviors and thermal enhancements with passive methods please refer to Ahmed et al. [7–9], Darzi et al. [10], Muhammed et al. [11], Kurtulmus et al. [12], and Aly et al. [13].

Active methods are another kind of heat transfer augmentation method. They need external power input for the heat transfer enhancement and supply greater flow mixing for this purpose. These techniques can develop more aggressive flow behavior compared to passive flow control techniques. The most popular active heat transfer improvement techniques in investigations are pulsating flow, acoustic waves, synthetic jets, injection and magnetic fields. Biswas et al. [14] presented an effective way to improve mixed convective heat transfer in a grooved channel with injection. According to them, performance with injection is always higher and heat transfer efficiency is observed to enhance from 50% to 218% depending on Reynolds number, *Re*, Richardson numbers, *Ri* and injection. According to Aly et al. [15], substantial heat transfer improvement can be acquired by the movement of circular cylinders in the fluid flow. Despite the existence of flow resistance of the porous substance in a cavity, the improvement in heat transfer using aspiration is remarkable. The magnitude of heat transfer improvement changes with respect to direction wall motion together with involved parameters [16]. For further studies on the hydrothermal behaviors and thermal enhancements with active methods please refer to Biswas et al. [17], Chakravarty et al. [18], Hamzah et al. [19], Zontul et al. [20].

Combining passive and active flow control techniques yields better outcomes in improving heat transfer efficiency. During the application of passive techniques in corrugated channels, corrugation surfaces are the weak locations with regard to heat transfer efficiency because of the low flow velocity caused by recirculation zones in corrugations. Utilizing an active technique enables the interaction between high flow velocity region and corrugation surface because of the removal of recirculation regions. Thus, the weakness of corrugated channels is eliminated and heat transfer efficiency is augmented compared to single employment of passive methods. Research including the simultaneous application of corrugated channels as a passive technique and magnetic field as an active technique have recently become very popular and the number of these studies is increasing day by day. Asadi et al. [21] studied the nonuniform magnetic field impact over 2D laminar convection heat transfer in a heat exchanger having sinusoidal corrugated walls. The results demonstrate that magnetic field application augments Nu_{avg} and also grows the pump work with a higher influence at a smaller *Re*. In the investigation of Heidary et al. [22], the thermal and flow characteristics of channels with wavy walls were studied for the presence of magnetic fields applied in the transverse direction to mainstream flow. Their computational findings revealed that the existence of both magnetic field and wavy wall at the same time is not appropriate for heat transfer improvement, any one of these flow control techniques is suitable for heat transfer augmentation. Aminfar et al. [23] performed numerical research about the impact of nonuniform magnetic field on the hydrothermal properties of a Fe_3O_4-water ferrofluid in the corrugated channel. Their computational results revealed that magnetic field implementation enhances the velocity of ferrofluid flow near the channel wall and this situation provides an enhancement in the heat transfer coefficient. According to Biswas et al. [24], with the increase in the intensity of the magnetic field, *Ha*, the buoyancy effect decreases significantly and hence causes a degradation in the heat transfer. Ahmed et al. [25] revealed that the heat transfer rate declined by 30.66% when Hartmann numbers augmented from $Ha = 0$ to $Ha = 50$ for ferroparticle volume fraction, $\Phi = 5\%$. Mei et al. [26] performed an experimental investigation to explore the hydrothermal behaviors of Fe_3O_4-water ferrofluid in a corrugated tube with a variety of magnetic field strengths. According to the presented results, the simultaneous applications of a nanofluid, magnetic field, and corrugated tube improve heat transfer rate remarkably at the small expense of increasing the flow resistance. Larimi et al. [27] revealed that the magnetic field is very impressive for improving Nu_{avg} inside heat exchangers, moreover, the maximum and minimum local Nusselt numbers, Nu_L in the rib region enhances with augmentation of magnetic field strength. The essential outcome in the investigation of Rashidi et al. [28] is that the velocity profile in the channel gets flatter and the velocity gradient raises in the vicinity of the wall with a growing Hartmann number, *Ha*. According to the outcomes of Ali et al. [29], the Nu_{avg} and entropy production grow by increasing the *Ra* and Φ while they attenuate with rising Hartmann number, *Ha*. Shaker et al. [30] revealed that a non-uniformly applied magnetic field alters hydrothermal behaviors and formed new vorticities in ferrofluid flow because of the Kelvin force impact. In the numerical work of Mousavi et al. [31], the influence of a nonuniformly applied magnetic field on flow and thermal characteristics inside the wavy corrugated channel is higher than in a channel with straight walls. According to Sachica et al. [32], entropy production due to the existence of a magnetic field weakens when

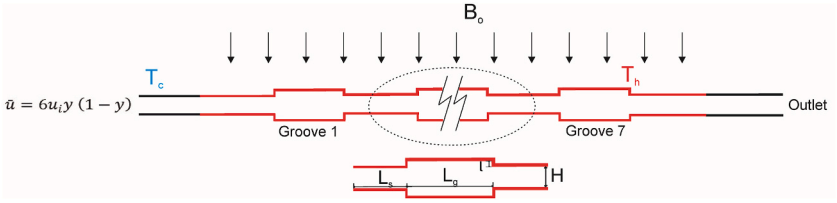

Fig. 1. Illustration of parameters describing the problem domain and grooved channel.

Φ grows for the whole considered *Ha*. They revealed that when the *Ha* changes, the system is subjected to many transitions. In the investigation of Mehrez et al. [33], it was revealed that the entropy production attenuates by growing the *Ha*. Selimefendigil and Oztop [34] revealed that the total entropy production rate attenuates for the horizontally oriented magnetic field, $¥ = 0^\circ$ which can be attributed to the repression of convection and slowing down the fluid movement by growing *Ha*. When the magnetic field inclination angles are, $¥ = 45^\circ$ and 90°, the entropy generation ratio gets higher. With increasing *Ha*, the maximum value of stream function and the intensity of the velocity field decrease due to increasing Lorentz force which opposes fluid motion at a higher *Ha* [35]. In the investigation of Biswas et al. [36] it was stated that the aspiration shows effective performance in heat transfer improvement under natural convection independent of magnetic field application. In addition, magnetic field applications remarkably control flow fields and temperature distributions. According to Dutta et al. [37], the Nu_{avg} attenuates by enhancing the *Ha*, especially at greater *Ra*, $Ra = 10^5$ and 10^6. In the investigation of Salehi et al. [38] it was stated that the growing *Ha* causes the velocity profile and thermal profile to be decreased. Liao and Li [39] reported that the increasing magnetic field intensity has a suppressive effect on natural convective flow, resulting in significant changes in thermal flow characteristics demonstrated by streamlines and isotherm contours. As a consequence, the average Nusselt number, Nu_{avg} and levels of maximum stream function, $S_{\max}$ decrease with increasing magnetic field intensity.

In this study, the impact of a uniform magnetic field on hydrodynamic, thermal, and entropy production properties of CuO-water nanofluid flow in the rectangular grooved channel is numerically investigated. The influences of many variables namely Reynolds numbers, *Re*, Hartmann numbers, *Ha* and volume fractions of nanoparticles, Φ on the hydrodynamic, thermal, and entropy generation properties are observed utilizing Fluent (version 20) program code.

2. Importance and novelty of investigation

Magnetohydrodynamics (MHD) is the study of fluid motion that involves the interaction between the fluid and an applied magnetic field. MHD flows are carried out in a wide range of engineering applications like flow meters, materials science, metallurgical process, and casting that include the interaction of the working fluid with the applied magnetic field. The other influential employment of MHD flow is the cooling circuits of fast fission reactors and self-cooled blankets of fusion reactors as reported by Morley et al. [40]. The combination of Maxwell's equations and the Lorentz force in the hydrodynamic momentum equation adds complexity and nonlinearity to MHD flow problems, making them both attractive and challenging for researchers.

To the best of the authors' observation, although it is probable to observe some investigations about magnetic field influence on hydrothermal characteristics in sinusoidal and trapezoidal corrugated channels, the research about influences of magnetic field on hydrothermal characteristics and entropy production of the rectangular grooved channel has not been previously published. Furthermore, considering the significance of entropy production in industrial and engineering applications, this study includes magnetic field impact on entropy production of CuO-water nanofluid flow inside the rectangular grooved channel, unlike the existing studies of magnetic field influence in sinusoidal and trapezoidal corrugated channels. The current investigation will become the first publication related to the uniform magnetic field which influences hydrodynamic, thermal, and entropy production properties of a nanofluid flow through the rectangular grooved channel with detailed works comprising the impacts of *Ha*, Φ and *Re*.

3. Numerical methodology

3.1. Problem description and governing formulations

This study numerically investigates heat transfer and nanofluid flow along rectangular grooved channels in the existence of uniform magnetic field. The problem domain comprises a channel with a phase angle of 180° having rectangular grooved upper and lower walls as demonstrated in Fig. 1. Grooved section of the channel includes seven grooves and there are straight sections with 150 mm upstream and 250 mm downstream of it. The channel height is equal to $H = 16$ mm. The aspect ratio which is the proportion of groove depth, l to channel height, H is taken as $l/H = 0.4$. The grooved section length is equal to $L_g = 60$ mm and the ratio of grooved section length, L_g to the straight section length, L_s is taken as $L_g/L_s = 1$. Copper oxide (CuO)-water nanofluid is considered as a coolant and its thermophysical properties of it assumed to be independent of temperature change. Flow is considered as two-dimensional, additionally, since Reynolds numbers are considered in the range of $250 \leq Re \leq 1250$, it is accepted as laminar. Reynolds numbers, *Re* are chosen in such a range because the previous studies in the literature stated that the magnetic field is more effective on laminar flow. Hartman numbers which is the parameter describing magnetic field strength are selected as $Ha = 0$, 8, 16 and 24. Since the recirculation flow zones in the grooves are almost completely suppressed and destroyed at $Ha = 24$, the Hartmann number is not taken as higher than $Ha = 24$. The Prandtl number which is the ratio of kinematic viscosity, ν to thermal diffusivity, α is taken as $Pr = 5.95$ in the simulations for $\Phi = 3\%$. Equations that govern the problem are given as follows [41,42];

Continuity

$$\frac{\partial \overline{u}}{\partial \overline{x}}+\frac{\partial \overline{v}}{\partial \overline{y}}=0 \tag{1}$$

X-momentum

$$\rho_{nf}\left(\frac{\partial \overline{u}}{\partial \overline{t}}+\overline{u}\frac{\partial \overline{u}}{\partial \overline{x}}+\overline{v}\frac{\partial \overline{u}}{\partial \overline{y}}\right)=\frac{-\partial \overline{p}}{\partial \overline{x}}+\mu_{nf}\left(\frac{\partial^2 \overline{u}}{\partial \overline{x}^2}+\frac{\partial^2 \overline{u}}{\partial \overline{y}^2}\right)-\sigma_{nf}B_0^2\,\overline{u} \tag{2}$$

Y-momentum

$$\rho_{nf}\left(\frac{\partial \overline{v}}{\partial \overline{t}}+\overline{u}\frac{\partial \overline{v}}{\partial \overline{x}}+\overline{v}\frac{\partial \overline{v}}{\partial \overline{y}}\right)=\frac{-\partial \overline{p}}{\partial \overline{y}}+\mu_{nf}\left(\frac{\partial^2 \overline{v}}{\partial \overline{x}^2}+\frac{\partial^2 \overline{v}}{\partial \overline{y}^2}\right) \tag{3}$$

Energy

$$(\rho Cp)_{nf}\left(\frac{\partial T}{\partial \overline{t}}+\overline{u}\frac{\partial T}{\partial \overline{x}}+\overline{v}\frac{\partial T}{\partial \overline{y}}\right)=k_{nf}\left(\frac{\partial^2 T}{\partial \overline{x}^2}+\frac{\partial^2 T}{\partial \overline{y}^2}\right) \tag{4}$$

The above equations are normalized by using the following expressions. During the *Re* calculation, twice the channel height, *H* is accepted as a reference length.

$$x=\frac{\overline{x}}{H}, y=\frac{\overline{y}}{H}, u=\frac{\overline{u}}{u_i}, v=\frac{\overline{v}}{v_i}, t=\frac{\overline{t}u_i}{H}, \theta=\frac{T-T_c}{T_h-T_c}, Pr=\frac{\nu_f}{\alpha_f}, p=\frac{\overline{p}}{\rho_f u_i^2}, Ha=B_0 2H\sqrt{\frac{\sigma_f}{\mu_f}}, Re=\frac{u_i 2H}{\nu_f} \tag{5}$$

Therefore non-dimensional form of governing Eqs. (1)–(4) are stated below;
Continuity

$$\frac{\partial u}{\partial x}+\frac{\partial v}{\partial y}=0 \tag{6}$$

X-momentum

$$\frac{\partial u}{\partial t}+u\frac{\partial u}{\partial x}+v\frac{\partial u}{\partial y}=-\frac{\rho_{bf}}{\rho_{nf}}\frac{\partial p}{\partial x}+\frac{\nu_{nf}}{\nu_{bf}}\frac{1}{Re}\left(\frac{\partial^2 u}{\partial x^2}+\frac{\partial^2 u}{\partial y^2}\right)-\left(\frac{\sigma_{nf}}{\sigma_{bf}}\right)\left(\frac{\rho_{bf}}{\rho_{nf}}\right)\frac{Ha^2}{Re}u \tag{7}$$

Y-momentum

$$\frac{\partial v}{\partial t}+u\frac{\partial v}{\partial x}+v\frac{\partial v}{\partial y}=-\frac{\rho_{bf}}{\rho_{nf}}\frac{\partial p}{\partial y}+\frac{\nu_{nf}}{\nu_{bf}}\frac{1}{Re}\left(\frac{\partial^2 v}{\partial x^2}+\frac{\partial^2 v}{\partial y^2}\right) \tag{8}$$

Energy

$$\frac{\partial \theta}{\partial t}+u\frac{\partial \theta}{\partial x}+v\frac{\partial \theta}{\partial y}=\frac{\alpha_{nf}}{\alpha_{bf}}\frac{1}{RePr}\left(\frac{\partial^2 \theta}{\partial x^2}+\frac{\partial^2 \theta}{\partial y^2}\right) \tag{9}$$

As shown in Fig. 1, magnetic field is applied in the vertical direction. Therefore, resulting Lorentz forces will take place in the *x*-direction. For this reason, effect of Lorentz forces on the flow is included in the calculation by adding a source term to the *x*-momentum equation. The Hartman number, *Ha* in source terms is the proportion of magnetic forces to viscous forces. Since the magnetic forces are a function of magnetic field strength, an increased *Ha* represents higher magnetic field strength.

In the current work, the thermal performance and enhancement in the rectangular corrugated channel are determined with the Nusselt number. The Nu_L through the heated wall of the rectangular corrugated channel can be given in Eq. (10) [43]:

$$Nu_L=-\left(\frac{k_{nf}}{k_{bf}}\right)\frac{\partial \theta}{\partial y} \tag{10}$$

The Nu_{avg} is calculated by integrating the above equation (Eq. 10) [43]:

$$Nu_{avg}=\frac{1}{L_w}\int_0^{L_w} Nu_L dL \tag{11}$$

where L_w represents the length of the rectangular corrugated wall.

3.2. Boundary conditions and nanofluid properties

In the current work, a no-slip boundary condition is implemented at channel walls (u = v = 0). Fixed heat flux is implemented on grooved walls but straight channels, located upstream and downstream of the grooved channel are adiabatic ($\partial\theta/\partial y = 0$). A fully developed velocity structure is described at the channel inlet as $u = 6y\,(1-y)$ and pressure at the domain outlet is adjusted as a value of zero (P = 0). Thermophysical features of nanofluid are determined by mathematical formulations below. In addition, CuO-water

Table 1
Properties of water and solid particles.

	ρ (kg/m^3)	C_p (J/kgK)	k (W/mK)	σ
Pure Water	998.2	4182	0.6	0.05
CuO	6500	540	18	2.7×10^8

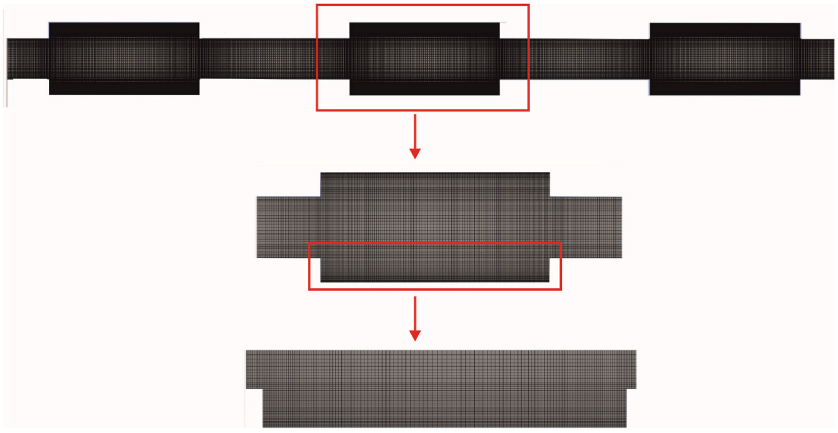

Fig. 2. Grid structure for all examined cases.

nanofluid is regarded for lower volume fractions, $\Phi = 3\%$ to prevent particle deposition and amalgamation. Thus, the single-phase model is appropriate to the current investigation and the lower Φ and particle diameter provide homogenous distribution of nanoparticles in the base fluid [44–46]. Biswas et al. [47] stated that thermo-physical features such as nanofluid thermal conductivity and viscosity and physical models are required to be selected accurately and precisely independent of the single or two-phase model. It is observed from the published papers that for nanoparticles with smaller sizes, the influences of drag, buoyancy, and gravity forces are insignificant on nanoparticles distribution [46,48,49]. The features of water and CuO nanoparticles used in the below equations are given in Table 1 [50–52].

$$\rho_{nf} = (1-\Phi)\rho_{bf} + \Phi\rho_{np} \tag{12}$$

$$\left(\rho C_p\right)_{nf} = (1-\Phi)\left(\rho C_p\right)_{bf} + \Phi\left(\rho C_p\right)_{np} \tag{13}$$

$$(\rho\beta)_{nf} = (1-\Phi)(\rho\beta)_{bf} + \Phi(\rho\beta)_{np} \tag{14}$$

$$\mu_{nf} = \frac{\mu_{bf}}{(1-\Phi)^{2.5}} \tag{15}$$

$$\frac{k_{nf}}{k_{bf}} = \frac{\left(k_{np}+2k_{bf}\right) - 2\Phi\left(k_{bf}-k_{np}\right)}{\left(k_{np}+2k_{bf}\right) + \Phi\left(k_{bf}-k_{np}\right)} \tag{16}$$

$$\sigma_{nf} = \sigma_{bf}\left(1 + \frac{3\left(\sigma_{np}/\sigma_{bf}-1\right)\Phi}{\left(\sigma_{np}/\sigma_{bf}+2\right) - \left(\sigma_{np}/\sigma_{bf}-1\right)\Phi}\right) \tag{17}$$

3.3. Numerical solution and mesh reliability

The numerical simulation of fluid flow, heat transfer, and entropy generation is performed using the Fluent (Version 20) program code. The simulation includes momentum source terms in Eqs. (2) and (3) to account for the impact of the uniform magnetic field on fluid flow and investigate how it affects heat transfer and entropy generation. These terms are incorporated into the simulation using the User Defined Functions (UDF) module. The simulation uses a SIMPLE (Semi-Implicit Method for Pressure-Linked Equations) scheme for the purpose of pressure and velocity coupling, with pressure interpolation at cell faces from cell center values performed using a second-order scheme. Convective terms discretization is done using the second-order upwind scheme technique, and temporal discretization is carried out with the second-order implicit model. The convergence criteria for the energy equation is set at 10^{-8}, while for momentum and continuity equations, it is set at 10^{-6}. Furthermore, the time step size used in the simulation is adjusted to 0.007 s, which ensures that the Courant number, *Cr*, is maintained at 0.6, satisfying the Courant-Lewy-Friedrich (CFL) condition in the smallest cell of the mesh at every time step.

Fig. 2 displays mesh structures in the rectangular grooved channel and detailed mesh distribution in the rectangular grooves and in

Table 2
Results of mesh independency test.

Element Number	Nu_{avg}	f
29,044	9.75	0.0681
43,566	9.559	0.06815
65,350	9.4178	0.06814
98,025	9.3246	0.06813
147,037	9.2552	0.06813
220,556	9.232	0.06813

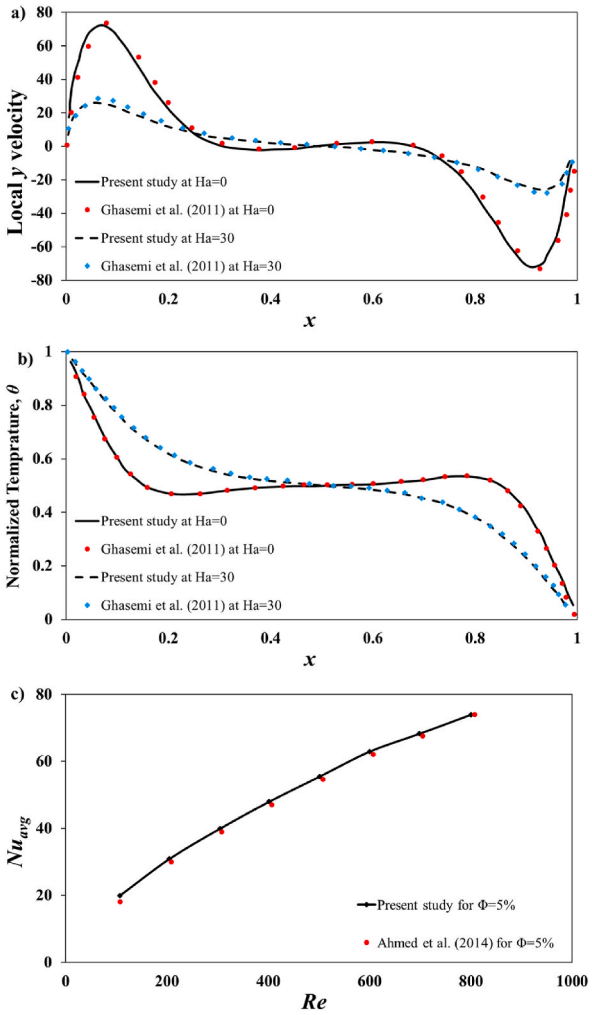

Fig. 3. (a–c) Comparison of a) local y velocity distribution b) temperature, θ for the case of uniform magnetic field implementation between current outcomes and numerical outcomes of Ghasemi et al. [54] at the middle of the square cavity for $Ra = 10^5$ and $\Phi = 3\%$ c) Nu_{avg}-Re curve with the study of Ahmed et al. [53] for the volume fraction of CuO nanoparticles, $\Phi = 5\%$.

the vicinity of channel walls. It can be observed from Fig. 2, the density of mesh distribution is greater in close regions of the upper and lower walls of the channel since velocity and temperature gradients are significant in these regions. The element number denoted in Table 2 is used for the grid independence test and one can observe from this table that 147,037 elements supply the best outcomes concerning computational cost-accuracy balance. According to Table 2, the uncertainty in Nu_{avg} is found as 0.082.

The solution technique used in the numerical simulation of the magnetic field is confirmed by comparing the results with a problem represented by Ghasemi et al. [30] at $Ha = 0$ and 30. As seen in Fig. 3 (a) and (b), the perfect consistency is acquired for the local distribution of y velocity and temperature, θ at the center of the square cavity under a uniform magnetic field. As illustrated in Fig. 3 (c), the change of Nu_{avg} with Re demonstrates very good agreement with the study of Ahmed et al. [53] used a similar geometry with the current study when the volume fraction of CuO nanoparticles is $\Phi = 5\%$. Thus, the observed great consistency between the

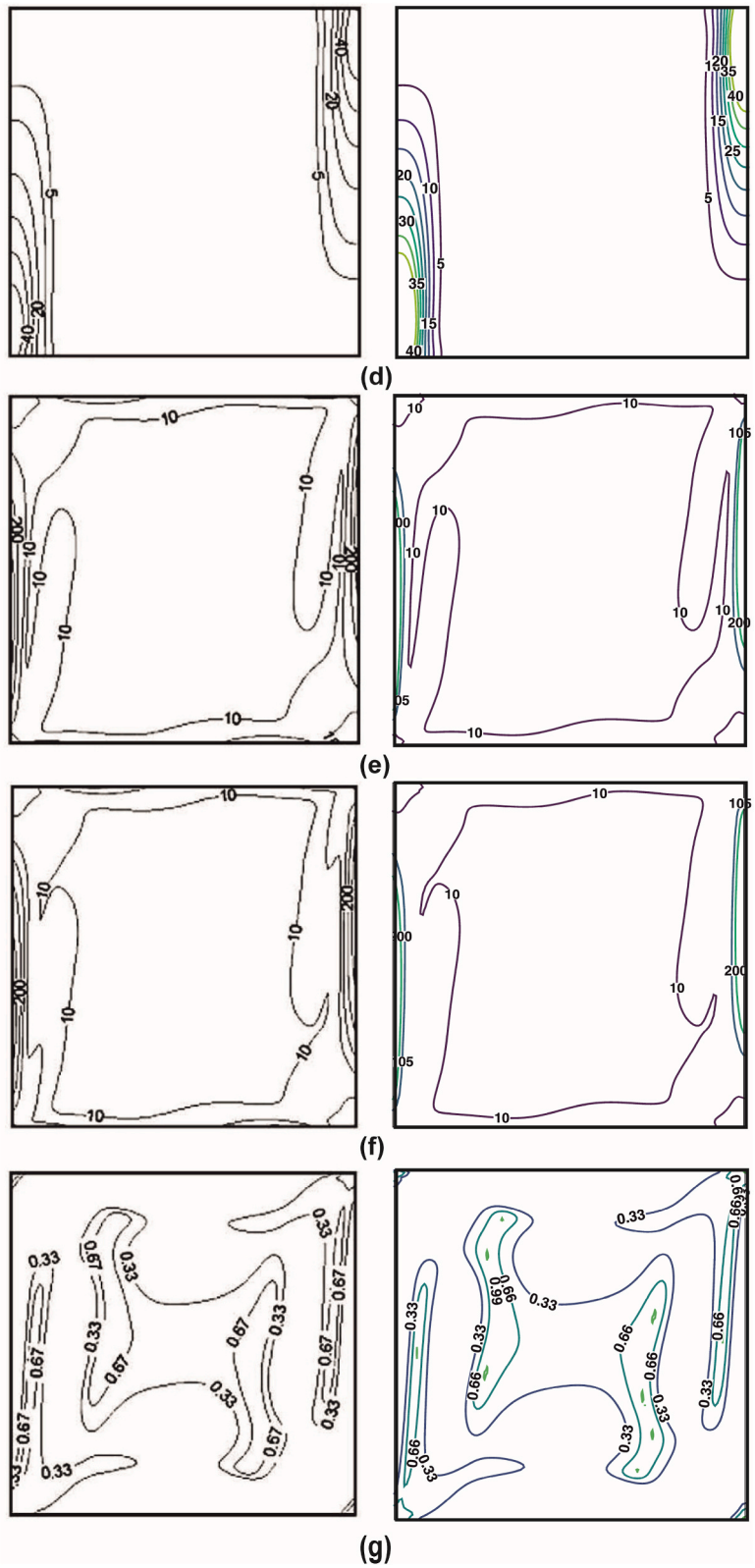

Fig. 3. (d–g) Comparison of the current entropy generation analysis technique (right column) with those present in the study of Ilis et al. [55] (left column) at $Ra = 10^5$. Notes: d) thermal entropy generation, s_{th} e) viscous entropy generation, s_{vis} f) total entropy generation, s_L g) Bejan number, *Be*.

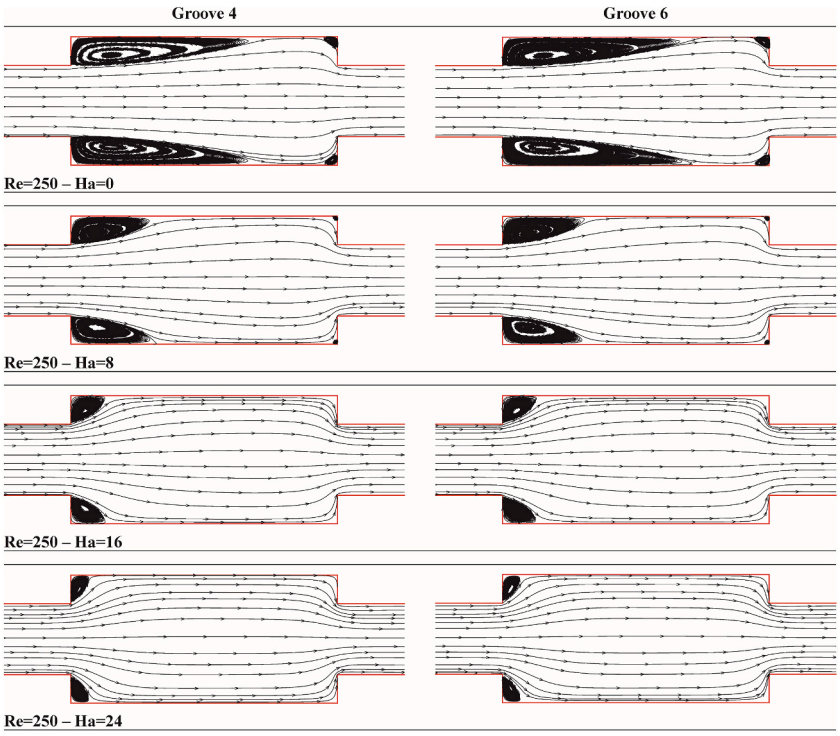

Fig. 4. (a) The magnetic field effects on the flow characteristics presented by patterns time-averaged streamlines in the rectangular grooved channel for Groove 4 and Groove 6 at $Re = 250$ with $\Phi = 3\%$.

outcomes of applied numerical code and available numerical data in the literature approves the trust in the present numerical study. As a result, the present CFD model can be safely used.

3.4. Entropy generation

Calculating the generation (or production) of entropy is a beneficial method to optimize the performance of thermal systems. For the present study, the entropy production because of the forced thermal convection of the nanofluid flow is determined by considering the effects of the thermal, viscous and applied magnetic sources. Accordingly, total entropy production, S_L results from the summation of these effects, which is written in a dimensional form as follows [43]:

$$\bar{s}_L = \bar{s}_{th} + \bar{s}_{vis} + \bar{s}_{mag} = \frac{k_{nf}}{T_o^2}\left[\left(\frac{\partial T}{\partial \bar{x}}\right)^2 + \left(\frac{\partial T}{\partial \bar{y}}\right)^2\right] + \frac{\mu_{nf}}{T_o}\left[2\left(\frac{\partial \bar{u}}{\partial \bar{x}}\right)^2 + 2\left(\frac{\partial \bar{v}}{\partial \bar{y}}\right)^2 + \left(\frac{\partial \bar{u}}{\partial \bar{y}} + \frac{\partial \bar{v}}{\partial \bar{x}}\right)^2\right] + \frac{\sigma_{nf}}{T_o} B_0^2\, \bar{u}^2 \tag{18}$$

where $T_o = \frac{T_h + T_c}{2}$.

In Eq. (18), the terms of $\bar{s}_{th}, \bar{s}_{vis}, \bar{s}_{mag}$ represent the effects of thermal, viscous, and magnetic fields on entropy production, respectively.

With help of non-dimensional parameters listed in Eq. (5), the non-dimensional configuration of Eq. (18) is described as follows:

$$s_L = s_{th} + s_{vis} + s_{mag} = \left[\left(\frac{\partial \theta}{\partial x}\right)^2 + \left(\frac{\partial \theta}{\partial y}\right)^2\right] + \left(\frac{\mu_{nf}}{\mu_{bf}}\right)\left(\frac{k_f}{k_{nf}}\right)\chi\left[2\left(\frac{\partial u}{\partial x}\right)^2 + 2\left(\frac{\partial v}{\partial y}\right)^2 + \left(\frac{\partial u}{\partial y} + \frac{\partial v}{\partial x}\right)^2\right] + \left(\frac{\sigma_{nf}}{\sigma_{bf}}\right)\left(\frac{k_f}{k_{nf}}\right) Ha^2 \chi u^2 \tag{19}$$

where, χ is an irreversible factor, and its definition is given below:

$$\chi = \frac{\mu_{bf} T_o}{k_{bf}}\left(\frac{u_i}{qL/k_{bf}}\right)^2 \tag{20}$$

The mean value of total entropy generation, S_L along a considered rectangular grooved channel is acquired by integrating Eq. (19) covering the entire flow domain:

$$S_{avg} = \frac{\int_A s_L dx dy}{A} \tag{21}$$

A comparison of the present entropy analysis technique with those present in the numerical study of Ilis et al. [55] is displayed in

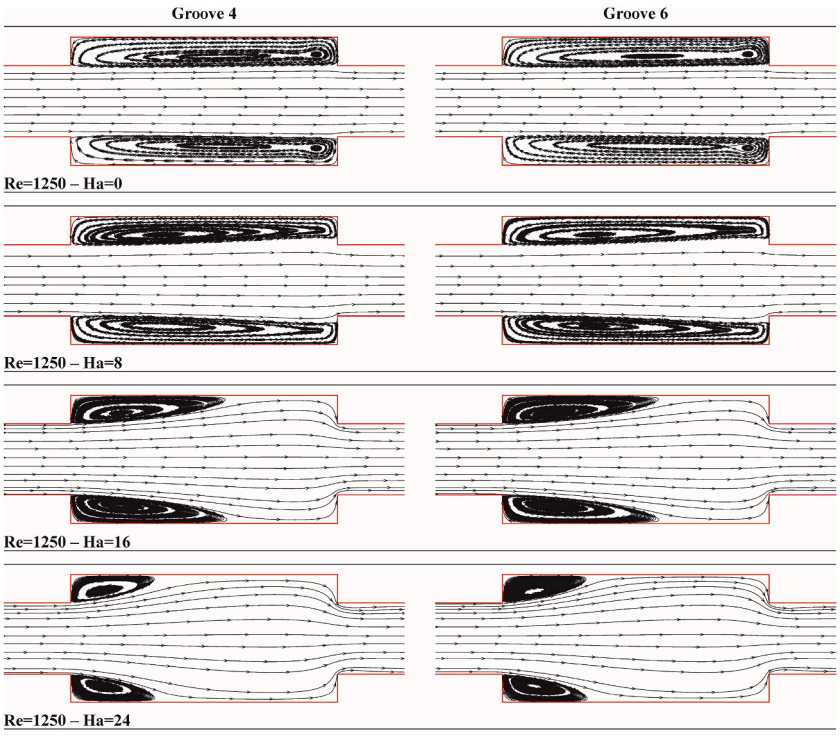

Fig. 4. (b) The magnetic field effects on the flow characteristics presented by patterns time-averaged streamlines in the rectangular grooved channel for Groove 4 and Groove 6 at $Re = 1250$ with $\Phi = 3\%$.

Fig. 3(d–g). As demonstrated in these figures, admissible consistency is obtained between these compared studies, which approves the accurate representation of the current entropy equations.

4. Results and discussions

4.1. Streamline and velocity distribution

Fig. 4 (a) and (b) show the influence of the magnetic field on flow structures presented by the time-averaged streamline patterns in the rectangular grooved channel at $Re = 250$ and 1250, respectively for $\Phi = 3\%$. Achieved conclusions demonstrated that implementing uniform magnetic fields with different intensities induces major changes in the streamline patterns. In Fig. 4 (a), it can be seen that when the Ha raises from $Ha = 0$ towards $Ha = 24$ progressively, extent of the flow recirculation region in the rectangular grooves diminishes. The suppression of recirculation flow regions in grooves lets the flow to penetrate into the groove and leaves the groove without rotation. According to the results of Fig. 4 (a), the amount of flow that penetrated into the rectangular groove is higher at $Ha = 24$ compared to the case of $Ha = 8$. So, it is apparent that the flow rate will be raised in the vicinity of corrugated walls by increasing the Hartmann number, Ha. At $Re = 250$, although the flow recirculation region is not completely suppressed, it is restrained to a very small zone in rectangular grooves for $Ha = 16$ and $Ha = 24$. The separated flow zone in rectangular grooves is the lowest at $Ha = 24$. According to Fig. 4 (a), the flow recirculation region does not cover the whole gap in rectangular grooves at $Re = 250$ and $Ha = 0$ since the Reynolds number, Re is not great enough and the low pressure regions are small which causes the emergence of small recirculation zone in rectangular grooves. But, in Fig. 4 (b), one can observe that the recirculation flow region occupies the whole gap in the rectangular groove, at $Re = 1250$ and $Ha = 0$ due to the increased inertia force at a higher Reynolds number, Re. Fig. 4 (b) depicts that when the Ha is rised from $Ha = 0$ to $Ha = 8$, no considerable change is detected in the streamline patterns and the recirculation region covers the whole gap in the rectangular groove similar to the case of $Ha = 0$ at $Re = 1250$. But the further increment in Hartmann numbers to $Ha = 16$ and then $Ha = 24$, leads to suppression of recirculation flow region in grooves. One of the main observations from Fig. 4 (a) and (b) is that the required Ha for the beginning of flow recirculation region suppression increases with the rise in Re. Because the extent of recirculation flow regions in the rectangular groove attenuates when Hartmann numbers grow from $Ha = 0$ to $Ha = 8$ at $Re = 250$ while there is almost no change in streamline pattern with increasing Hartmann numbers from $Ha = 0$ to $Ha = 8$ at $Re = 1250$. At high Reynolds numbers, Re due to the strong inertia effect of mainstream flow, the uniform magnetic field has less influence on the flow characteristics in the rectangular grooved channel than at smaller Reynolds numbers, Re.

Lorentz forces which are known as resistive forces take place as a result of magnetic field implementation in the rectangular grooved channel. Lorentz forces are influential on a fluid carrying density in a magnetic field [43]. They slow down the nanofluid flow motion and behave like opponent body forces. The weakening of the recirculation zone in the rectangular grooves with the uniform magnetic field can be attributed to the magnetic field induced Lorentz forces which cause suppression of nanofluid flow, supply flow

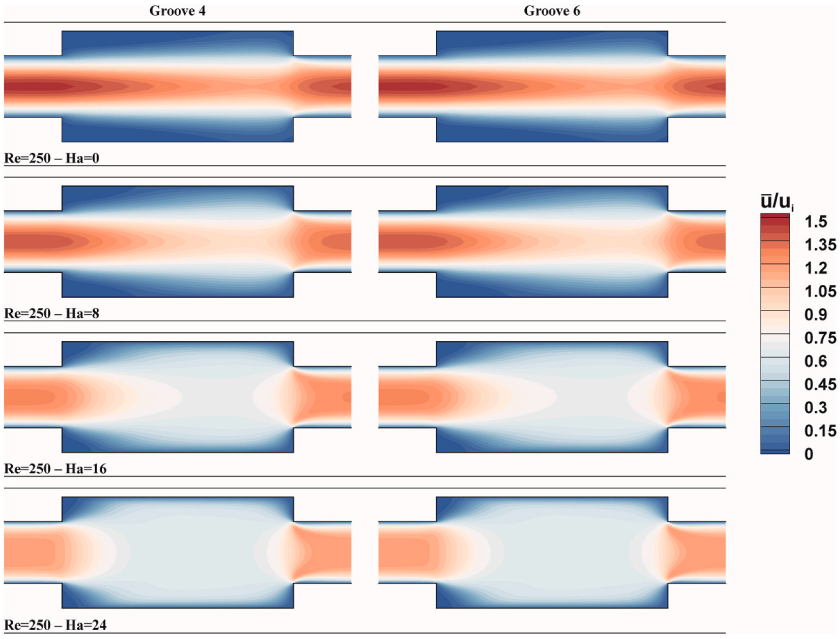

Fig. 5. (a) Effects of the magnetic field on the variation of normalized streamwise velocity distributions in the rectangular grooved channel for Groove 4 and Groove 6 at $Re = 250$ with $\Phi = 3\%$.

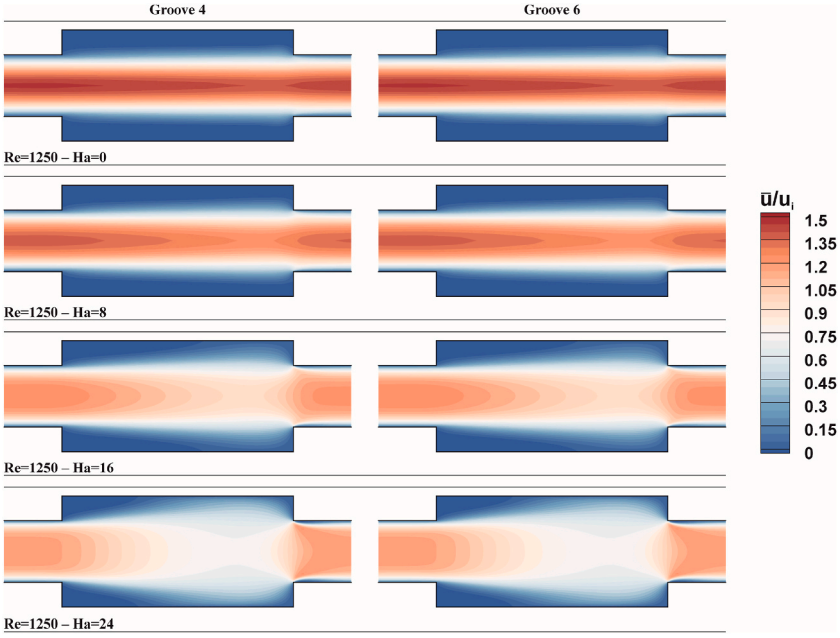

Fig. 5. (b) Effects of the magnetic field on the variation of normalized streamwise velocity distributions in the rectangular grooved channel for Groove 4 and Groove 6 at $Re = 1250$ with $\Phi = 3\%$.

stability, and act like damping forces that diminish instabilities in the flow zone. As a result, one way to weaken the flow recirculation region in rectangular grooved channels is to apply the uniform magnetic field. The repression of flow recirculation region in rectangular grooved channels is an effective situation from the points of flow behaviors and heat transfer performance since it increases heat transfer because of the conveying of more cold fluid to grooves which will be discussed in the following sections.

The effect of uniform magnetic field implementation on the flow characteristics revealed by variation of normalized streamwise velocity contours is demonstrated in Fig. 5 (a) and (b) at $Re = 250$ and 1250, respectively for $\Phi = 3\%$. The results demonstrated that the velocity gradient near walls enhances by raising the Ha so the extent of vorticity close to walls diminishes at both Reynolds numbers,

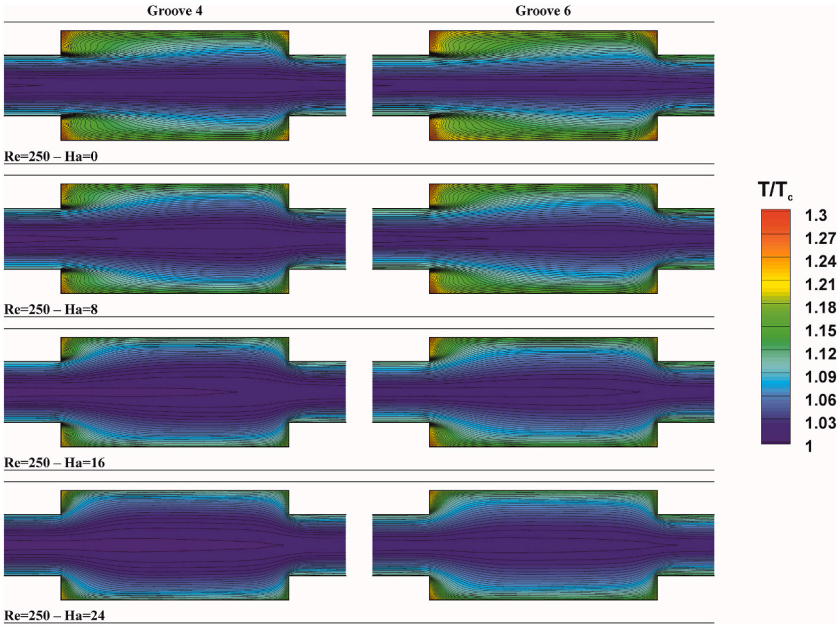

Fig. 6. (a) The magnetic field impacts on normalized temperature distributions and isotherm lines in the rectangular grooved channel for Groove 4 and Groove 6 at $Re = 250$ with $\Phi = 3\%$.

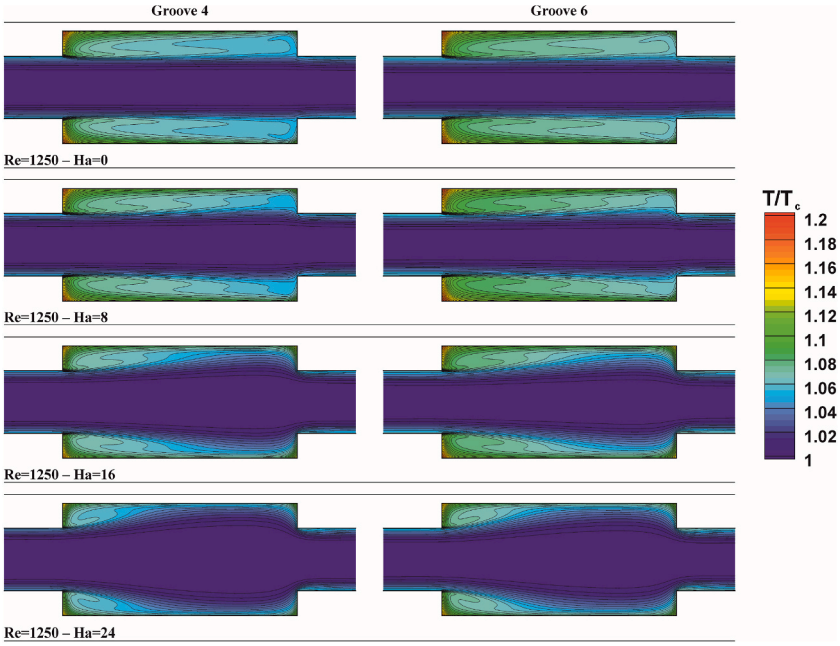

Fig. 6. (b) The magnetic field impacts on normalized temperature distributions and isotherm lines in the rectangular grooved channel for Groove 4 and Groove 6 at $Re = 1250$ with $\Phi = 3\%$.

$Re = 250$ and 1250. Because Lorentz forces caused by the application of a uniform magnetic field attenuate flow velocity at the channel center and by regarding fixed mass flow throughout the channel, the velocity of nanofluid flow substantially enhances in the vicinity of heated walls. This situation grows the velocity gradient and temperature gradient near the hot walls and heat transfer between heated walls and nanofluid flow enhances. An increment in the Ha augments mass flow rate and velocity gradient in the vicinity of hot walls providing greater heat diffusion throughout the wall and smaller wall temperature which enhances heat transfer efficiency and the Nu_{avg}. Furthermore, one can observe from Fig. 5 (a) and (b) that the velocity profile gets flatter with amplifying magnetic field intensity at both Reynolds numbers, $Re = 250$ and 1250. The extent of separated flow regions in rectangular grooves gets smaller in size while

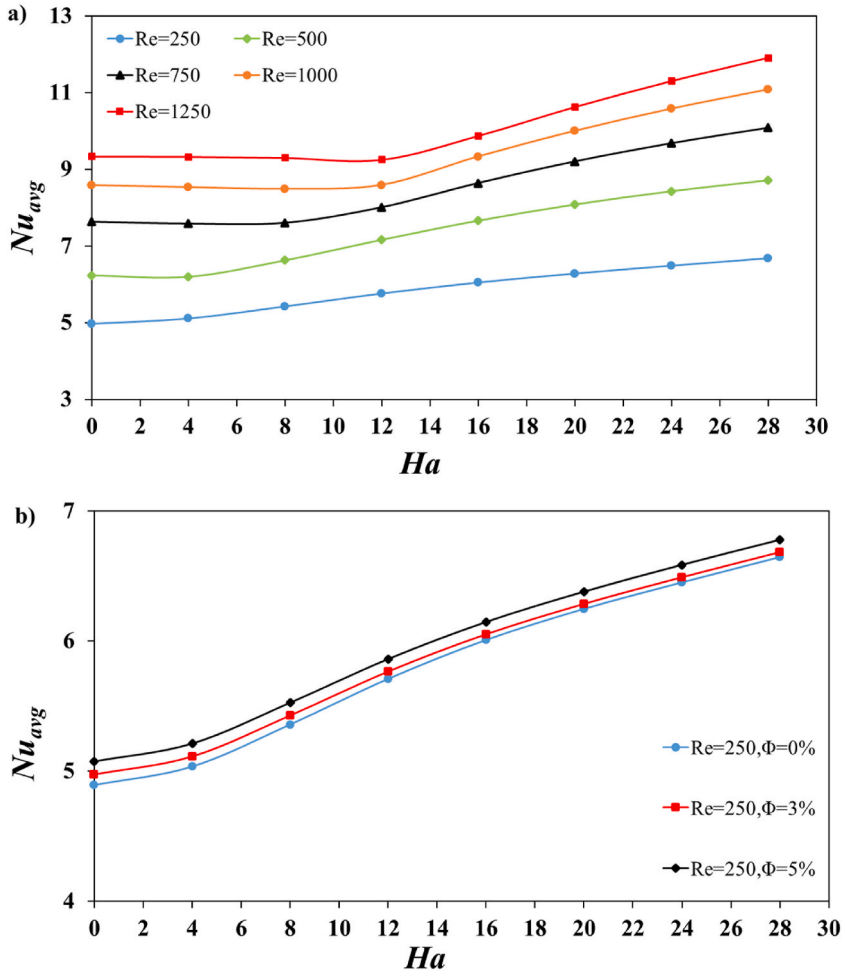

Fig. 7. The magnetic field effects on the Nu_{avg} variations a) at Reynolds number in the range of $250 \leq Re \leq 1250$ for $\Phi = 3\%$ b) at the Reynolds number, $Re = 250$ for $\Phi = 0\%$, 3% and 5%.

the Ha progressively augments from $Ha = 0$ towards $Ha = 24$. However, as the magnetic field strength increases, the situation that separated flow regions occupy a smaller zone within rectangular grooves is more effective at $Re = 250$ than $Re = 1250$. Because, at $Re = 1250$, the uniform magnetic field is less effective over flow structures in rectangular grooves due to the vigorous inertia effect of nanofluid flow compared to the Reynolds number, $Re = 250$.

4.2. Heat transfer analysis

The uniform magnetic field effect on normalized temperature distributions, T/T_c in the rectangular grooved channel is demonstrated in Fig. 6 (a) and (b) at $Re = 250$ and 1250, respectively. These figures reveal that applying a uniform magnetic field in a direction is very impressive on changes in temperature distribution and isotherm lines in the rectangular grooved channel. It can be seen that as the Ha progressively augments from $Ha = 0$ towards $Ha = 24$, the thermal boundary layer in the rectangular grooves gets thinner at both Reynolds numbers, $Re = 250$ and 1250. Furthermore, the temperature gradient in close regions of heated walls increases when the magnetic field is uniformly applied in the transverse direction. It is due to the direct contact of heated walls and cold flow which induces a great temperature gradient near heated walls. This situation also augments the heat transfer rate and the Nu_{avg} in the rectangular grooved channel by the existence of a uniform magnetic field. For the nonexistence of a uniform magnetic field, $Ha = 0$ at $Re = 250$ and 1250, the flow recirculation zone in the rectangular grooves obstructs the direct contact of the main cold flow with heated walls. The greater magnetic field strength is related to smaller wall temperature because of the rise in mass flow rate and velocity gradient in close regions to the wall thus heat diffusion enhances in the vicinity of the heated wall. This observation (reduction in the temperature of the wall) can be employed in the cooling of the industrial equipment and sensitive electronic components [12]. As it is clear from Fig. 6 (a) and (b), increasing Re from 250 to 1250 results in a reduction in the thermal boundary layer thickness within rectangular grooves, for a given Hartmann numbers, Ha. This trend implies that the Nusselt number, Nu_{avg} and the heat transfer rate increase as the Reynolds number increases. When these two figures are carefully examined, especially in Fig. 6 (b), one can say that the normalized temperature distribution, T/T_c in Groove 6 is higher than in Groove 4. Because the temperature of the nanofluid

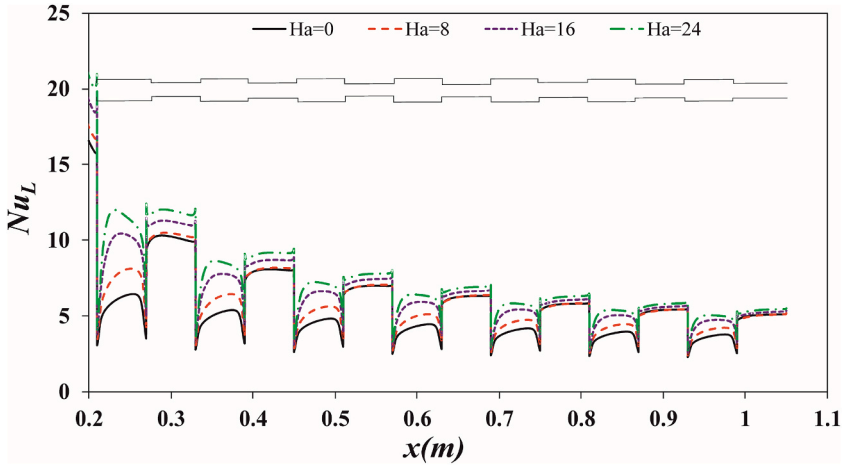

Fig. 8. The magnetic field influences on variations of the Nu_L at $Re = 250$ for the $\Phi = 3\%$ in the rectangular grooved channel.

enhances after passing through each groove due to the direct contact of the nanofluid with the heated wall in each groove.

Fig. 7 (a) demonstrates the effect of a uniform magnetic field on changes of the Nu_{avg} at Re within the range of $250 \leq Re \leq 1250$ for $\Phi = 3\%$. According to the results, the Nu_{avg} augments as the intensity of the uniformly applied magnetic field grows. For example, at $Re = 250$, the Nu_{avg} improves from $Nu_{avg} = 4.976$ at $Ha = 0$ to $Nu_{avg} = 5.428$ and 6.49 at $Ha = 8$ and 24, respectively. On the other hand, at $Re = 1250$, the Nu_{avg} increases sligtly from $Nu_{avg} = 9.328$ at $Ha = 0$ to $Nu_{avg} = 9.336$ at $Ha = 8$, and hence the Nu_{avg} increases significantly to $Nu_{avg} = 11.3$ at $Ha = 24$. This indicates that the magnetic field enhances the heat transfer rate especially at lower Reynolds numbers, Re and higher Hartmann numbers, Ha. Obtained results demonstrated that the Nu_{avg} augments approximately 9.08% for $Ha = 8$ and also it increases by 30.42% for $Ha = 24$ at $Re = 250$. In the case of $Re = 1250$ the Nu_{avg} improves by 0.087% for $Ha = 8$ and by 21.13% for $Ha = 24$ compared to the nonexistence of uniform magnetic field application case, where the Ha is zero. It can be said that at greater Re due to the high inertia influence of the main flow, the uniform magnetic field has less influence on the Nu_{avg} since the Nu_{avg} enhancement ratio due to the rise in the Ha is higher at $Re = 250$ than $Re = 1250$. The Nu_{avg} augmentation with a uniform magnetic field can be attributed to the situation that applying a uniform magnetic field suppresses the flow recirculation zones in the rectangular grooves and thus main cold flow can penetrate into the rectangular grooves. As a result, the velocity and temperature gradients enhance, and thermal boundary layers get thinner in the vicinity of heated walls in rectangular grooves which enhances the heat transfer rate and the Nu_{avg} by growing the Ha. Another important observation from Fig. 7 (a) is that the Nu_{avg} augments with an increase in the Re. For example, in Fig. 7 (a), at $Re = 500$ the Nu_{avg} is observed as $Nu_{avg} = 6.235$ and 8.430 for $Ha = 0$ and 24, respectively, however, at $Re = 1000$ the average Nusselt number is enhanced to levels of $Nu_{avg} = 8.584$ and 10.587 for $Ha = 0$ and 24, respectively. This indicates that the percentage enhancement of Nu_{avg} corresponds to 37.66% and 25.58% at $Ha = 0$ and 24, respectively, as the Re increases from $Re = 500$ to $Re = 1000$. The enhancement of Nu_{avg} because of the increment in Re can be attributed to the greater velocity of nanofluid flow and convection heat transfer rate. The convective transport structure enhances for the greater nanofluid velocities. Additionally, as explained in Fig. 6, the thickness of the thermal boundary layer decreases with the increment in Re which makes Nu_{avg} to be enhanced.

In Fig. 7 (b), it is expected that the inclusion of CuO nanoparticles in water with volume concentrations of, $\Phi = 3\%$ and 5% enhances the Nu_{avg} for all examined values of Ha at $Re = 250$. Obtained results demonstrated that in the absence of a magnetic field ($Ha = 0$) increasing the Φ from $\Phi = 0\%$ to $\Phi = 5\%$ gives rise a 3.71% increase in the average Nusselt number, Nu_{avg} augmentation. However, when the Ha increases to 8, 16, and 24, the values of Nu_{avg} enhancement are 3.13%, 2.3%, and 2.09%, respectively. The enhancement of Nu_{avg} due to an increase in volume concentrations, Φ can be attributed to the increased thermal conductivity, k of the nanofluid, and more severe Brownian movement of CuO nanoparticles compared to the pure water. The weakening thermal resistance induced by enhancing the volume fraction of nanoparticles (growing thermal conductivity) is useful for heat transfer and average Nusselt number, Nu_{avg} improvement. Furthermore, the Brownian motion of CuO solid particles can attenuate the thermal resistance of heat transfer between heated walls in the channel and water-CuO nanofluids which is effective on the Nu_{avg} improvement.

Fig. 8 represents the influence of the magnetic field on the Nu_L for $\Phi = 3\%$ in the rectangular grooved channel at $Re = 250$. As it is apparent in the figure, the Nu_L is enhanced as the magnetic field is uniformly implemented and its intensity gets higher along the rectangular grooved channel at the Reynolds number, $Re = 250$. When Hartmann numbers progressively increase from $Ha = 0$ towards $Ha = 24$, the Nu_L is distributed with greater values along the grooved channel. It should be noted that the value of Nu_L is greater on the straight section of the heated wall compared to the grooved section of the heated wall for all examined Ha. The reason for this is that, in the straight section of the heated wall, there is direct contact between the wall and the main cold nanofluid flow which induces a higher temperature gradient, leading to an enhancement in heat transfer rate and the Nusselt number, Nu_L. Utilizations of the magnetic fields generate energetic hydrodynamic vorticities that persist along the straight channel section between the grooves, thereby enhancing the mass and momentum exchange. As a result, heat transfer improvement is sustained while experiencing less pressure loss in the straight duct sections. This leads to higher thermal performance of the straight duct section compared to the corrugated section of the duct. On

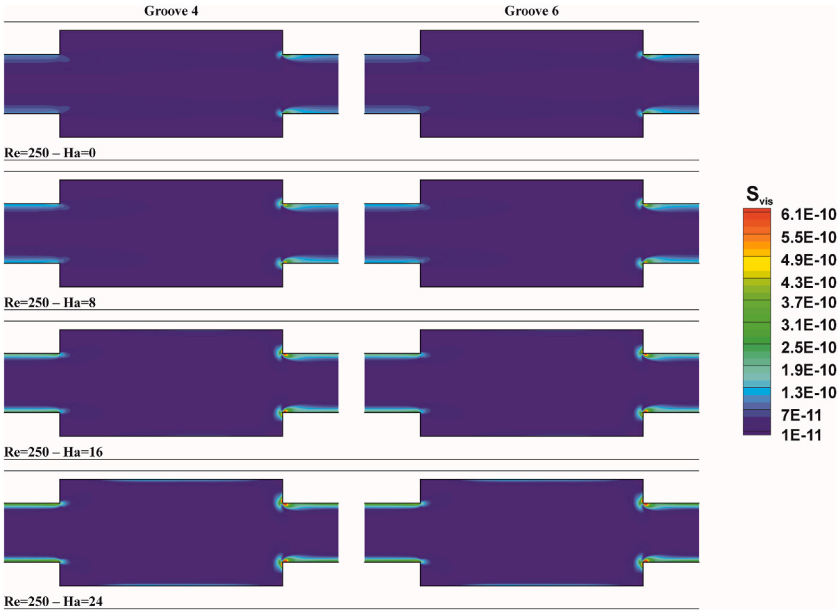

Fig. 9. (a) Influences of the magnetic field on the viscous entropy generation, S_{vis} across flow domain at the Reynolds number, $Re = 250$ with $\Phi = 3\%$.

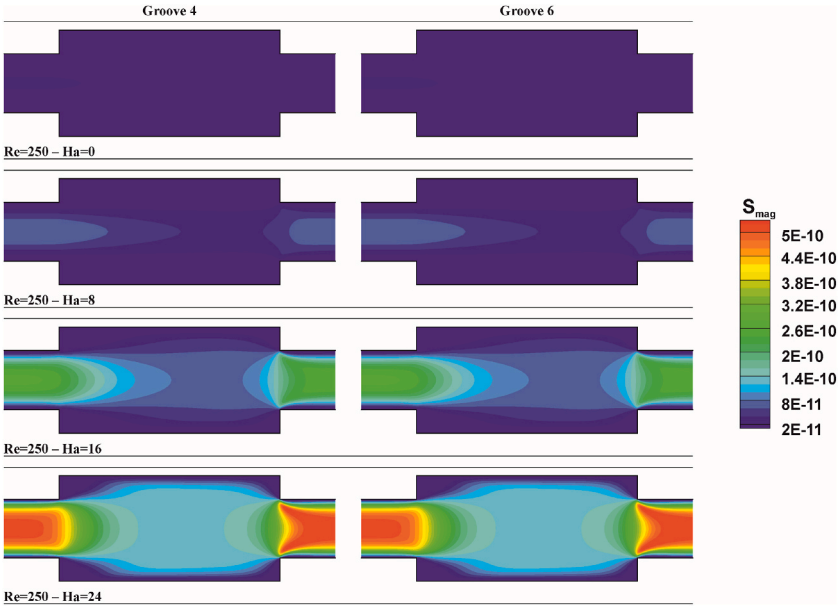

Fig. 9. (b) Influences of the magnetic field on the magnetic entropy generation, S_{mag} at the Reynolds number, $Re = 250$ with $\Phi = 3\%$.

the other hand, in the grooved section of the heated wall, the recirculation flow zone restrains the contact of the wall surfaces with the main cold flow, which leads to decrease in Nu_L. Furthermore, Nu_L deteriorates in the downstream direction due to the increasing temperature of the main flow after passing each groove. Increasing temperatures of the main flow reduces the heat exchange rate since heated walls come into contact with a higher temperature main flow instead of a colder one. The findings show that the difference in the distribution of Nu_L between grooves in flow direction diminishes because of the developing thermal boundary layer in the flow direction for all examined *Ha* and *Re*.

4.3. Entropy analysis

As already mentioned, analytical quantification of entropy production determines irreversible processes. A reduction in entropy production corresponds to an increase in thermal performance. Therefore, the characterization of irreversible processes through the investigated channel points directly to a precise statement of hydrothermal performance. As seen from Fig. 9 (a), (b) and (c), the

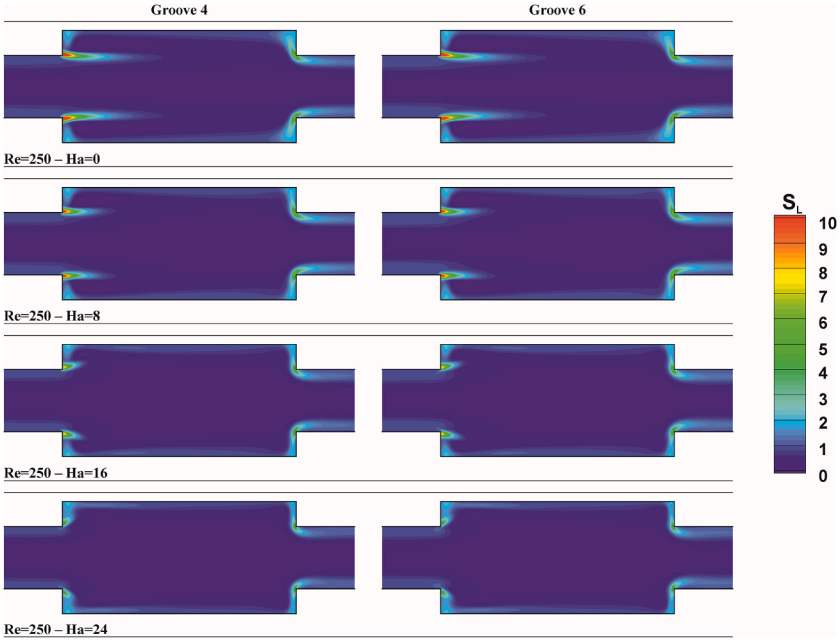

Fig. 9. (c) Influences of the magnetic field on the S_L production, at the $Re = 250$ with $\Phi = 3\%$.

contribution of magnetic, S_{mag} and viscous, S_{vis} entropy generations to the total entropy generation, S_L are very low and thus the thermal entropy generation, S_{th} is the most important component of the total entropy generation, S_L. The applied magnetic field affects the thermal entropy generation, S_{th} by changing the flow and thermal distributions in the rectangular corrugated channel. Therefore, it should not be thought that the increase in magnetic, S_{mag} and viscous, S_{vis} entropy production with the applied magnetic field will have a negative effect on the heat transfer performance. The situation that directly affects the heat transfer efficiency is the variation of the total entropy production, S_L with the applied magnetic field.

Fig. 9 (a) presents the impact of various intensities of magnetic field on the variation of viscous entropy, S_{vis} generation for the Groove 4 and Groove 6 of the considered channel at $Re = 250$ for the nanoparticles volume fraction, $\Phi = 3\%$. The patterns of S_{vis} clearly revealed that the high level of viscous entropy, S_{vis} generation extends alongside the straight walls of the convergent sections. This behavior is associated with high values of velocity gradients in these regions, as shown in Fig. 5 (a). In addition, it is worth noting that the entropy production due to the frictional effect of the working fluid flow is almost not generated within the remaining flow domain of the channel. This is directly related to the low-velocity gradients within these regions. As expected, the maximum level of viscous entropy, S_{vis} generations appear close to the right sharp angle of each groove of the tested channel, where the sudden contraction leads to the highest values of velocity gradients. At a fixed value of Reynolds numbers, the production of viscous entropy, S_{vis} gradually increases with an increase in the value of Hartmann numbers, Ha.

Fig. 9 (b) depicts influences of the magnetic field on variations in the magnetic entropy, S_{mag} generation at $Re = 250$ for $\Phi = 3\%$. As written in the last term of total entropy production equation (Eq. 19), magnetic entropy is an increasing function of both the velocity magnitude and Hartmann numbers, Ha. Therefore, for all the considered cases, there is no entropy generation due to the magnetic impact adjacent to the solid walls of the channel where no-slip boundary conditions are assumed for these walls. Moreover, the results reveal that the generation of the entropy, S_{mag} because of the magnetic influence significantly increases by enhancing the value of Ha. For $Re = 250$ at $Ha = 8$, the high-level zone of magnetic entropy, S_{mag} production occurs within the core flow of the convergent and divergent sections. By increasing the Ha to the value of 16, the high level of magnetic entropy, S_{mag} spreads to cover a half of the divergent grooves for $Re = 250$. At the highest intensity of the applied magnetic field ($Ha = 24$), this level of entropy extends to cover most regions of divergent grooves for $Re = 250$. As already mentioned, this type of entropy is directly related to the velocity distribution of the flow region. Accordingly, these behaviors of the magnetic entropy, S_{mag} are consistent with those shown in the velocity distributions shown in Fig. 5 (a).

Fig. 9 (c) represents local production of total entropy, S_L under different values of the Ha at $Re = 250$, for the $\Phi = 3\%$. For the current corrugated channel, the total entropy production by nanofluid flow happens essentially because of the effects of heat transfer, frictional flow, and magnetic source. Therefore, Fig. 9 (c) defines the summation of thermal, S_{th} viscous, S_{vis} and magnetic entropy, S_{mag} generations for $Re = 250$. As can be seen from these patterns of S_L, all the presented cases indicate that the high level of S_L generation spreads along the solid walls of the channel. This is caused by high-temperature gradients in those regions, as demonstrated in Fig. 6. It is worth noting that the S_L generation is almost non-existent along the central flow region of the channel. This is directly related to the uniform temperature distribution within this region, as presented in the isothermal contours. Furthermore, a low level of total entropy, S_L is observed in each rectangular groove along the corrugated channel. As portrayed in Fig. 4 (a), a flow recirculation zone emerges within each groove. This flow recirculation precludes the connection between the cold fluid and the heated walls, thus reducing

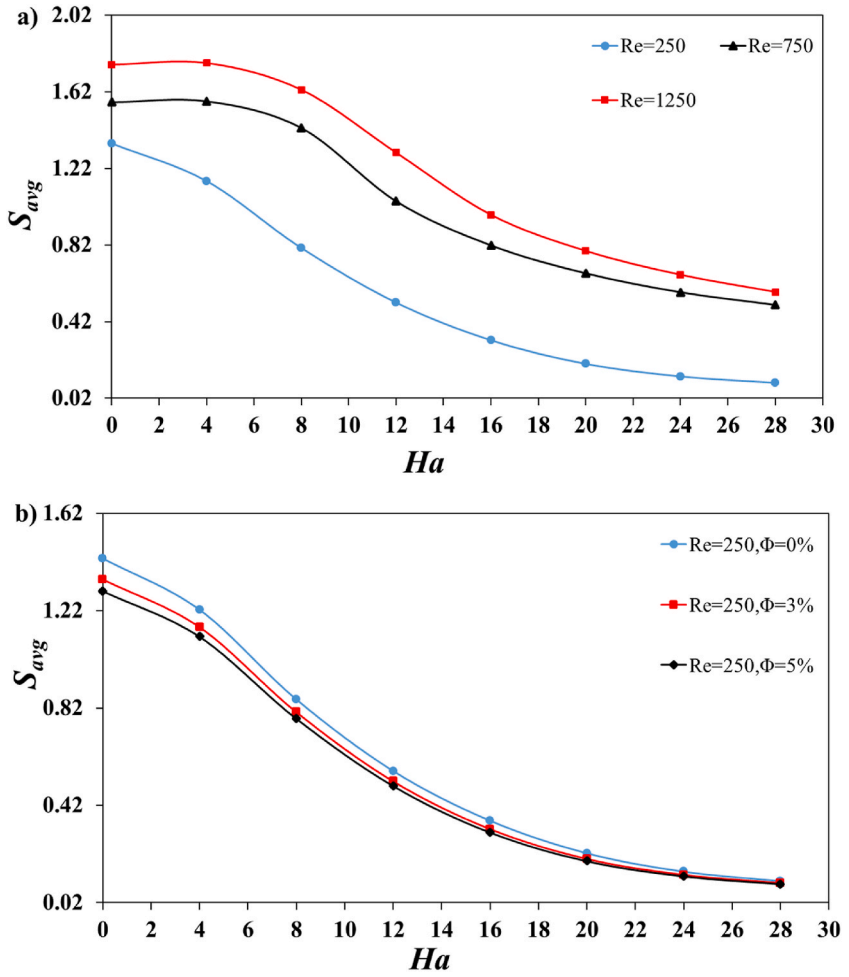

Fig. 10. The magnetic field effects on the S_{avg} a) at Re = 250, 750 and 1250 for Φ = 3% b) at the Re = 250 for Φ = 0%, 3% and 5%.

temperature gradients. Accordingly, the generation of total entropy, S_L drops significantly in these regions. Furthermore, the maximum amount of total entropy, S_L is generated near the left sharp edge of each groove. For a given Reynolds number, Re the total entropy, S_L production inside the channel diminishes as the intensity of magnetic field rises (i.e., increasing Hartmann numbers, Ha). This implies that the applied magnetic source attenuates the generation of total irreversibility in corrugated channels.

Fig. 10 (a) exhibits the variation of the average total entropy production, S_{avg} for a fixed nanoparticle volume fraction of Φ = 3% and different ranges of the Reynolds number, Re, and Hartmann number, Ha. The results of this figure provide useful details for understanding the basic effects of fluid flow structure and magnetic fields on the overall entropy, S_{avg} production within rectangular corrugated channels. It can be obviously observed that the total entropy, S_{avg} grows as the Reynolds number, Re gets higher. For instance, at Ha = 0, the amount of total entropy, S_{avg} increases by about 31% by rising the Re from Re = 250 to Re = 1250. In addition, this increment is observed to be about 103% when the magnetic field is applied with a strength of Ha = 8. This situation can be attributed that the increment in Re causes an augmentation of both velocity and temperature gradients through the flow field and, thus, leads to further generation of entropy. For a given value of Re it can be observed that the S_{avg} diminishes sharply after Ha>8. This is due to the significant effect of high magnetic field intensity on both flow hydrodynamics and thermal distributions.

Fig. 10 (b) demonstrates the impacts of magnetic source strength and CuO nanoparticles concentration on the S_{avg} for Re = 250. Numerous investigations have informed that there is little variation in the hydrothermal features between host fluids and nanofluids [4]. This attributed to the fact that changes in thermophysical properties have an insignificant effect on hydrothermal behavior compared to changes in operating and boundary conditions. Based on the results presented in Fig. 10 (b), it can be observed that increasing the concentration of CuO nanoparticles in the base liquid leads to a slight decrease in the average total entropy generation, S_{avg}. It is possible to detect differences in the S_{avg} value with respect to changes in the CuO concentrations for Re = 250, but this difference fades with an enhancement in the magnetic field intensity field subjected to the channel. This is because increasing the magnetic field strength reduces the differences in temperature gradients, thereby reducing the influence of the thermal properties.

5. Conclusions

In this numerical study, the effects of a uniformly applied magnetic field on the hydrothermal characteristics of a nanofluid consisting of water and CuO inside a rectangular grooved channel were investigated. The current investigation becomes the first study associated with the uniform magnetic field impact on the thermal, flow and entropy generation behaviors of a nanofluid in a rectangular grooved channel with extensive analysis comprising the impacts of together Hartmann numbers, *Ha*, Reynolds numbers, *Re* and volume fractions of nanoparticles, Φ. The most important results are demonstrated as follows.

- The extent of the flow recirculation region in rectangular grooves diminishes with the application of a uniform magnetic field at $Re = 250$ and 1250.
- The uniform magnetic field application reduces the thermal boundary layer in rectangular grooves and increases the temperature gradient in close regions of heated walls which makes Nu_{avg} to be augmented.
- The increment in Hartmann number, *Ha* causes smaller wall temperature due to the rise in mass flow rate and velocity gradient in close regions to the wall thus heat diffusion enhances in the vicinity of the heated wall.
- At a Hartmann number of $Ha = 0$, the average Nusselt number is observed to be $Nu_{avg} = 4.976$. However, this value improves to $Nu_{avg} = 5.428$ and 6.49 for Hartmann numbers of $Ha = 8$ and 24, respectively. This corresponds to a 9.08% increase in Nu_{avg} for $Ha = 8$ and a 30.42% increase in Nu_{avg} for $Ha = 24$, compared to the case with no magnetic field (i.e., $Ha = 0$) at a Reynolds number of $Re = 250$.
- Increasing the volume concentration of CuO nanoparticles, Φ improves the Nu_{avg} for all examined Hartmann numbers, *Ha* at $Re = 250$.
- For a given *Re,* it can be detected that total entropy generation decreases substantially when the Hartmann number exceeds 8 (i.e., $Ha>8$). This is due to the significant impact of the high magnetic field intensity on the flow characteristics and thermal distributions together.

CRediT authorship contribution statement

Sergen Tumse: Investigation, Methodology, Writing, Review, Simulations and Editing, **Besir Sahin:** Investigation, Methodology, Review, Supervision and Editing.

Declaration of competing interest

The authors declare that they have no known competing financial interests or personal relationships that could have appeared to influence the work reported in this paper.

Data availability

Data will be made available on request.

Acknowledgments

This study is supported by the Scientific Researched Project Office of Çukurova University under contract no: FDK-2021-13879.

References

[1] H. Zontul, B. Şahin, Experimental investigation of convective heat transfer performance and hydrodynamics of pulsating flow through the rectangular grooved channel, Exp. Therm. Fluid Sci. 141 (2023), 110796, https://doi.org/10.1016/j.expthermflusci.2022.110796.
[2] N. Tokgoz, M.M. Aksoy, B. Sahin, Investigation of flow characteristics and heat transfer enhancement of corrugated duct geometries, Appl. Therm. Eng. 118 (2017) 518–530, https://doi.org/10.1016/j.applthermaleng.2017.03.013.
[3] H. Zontul, H. Hamzah, N. Kurtulmuş, B. Şahin, Investigation of convective heat transfer and flow hydrodynamics in rectangular grooved channels, Int. Commun. Heat Mass Tran. 126 (2021), 105366, https://doi.org/10.1016/j.icheatmasstransfer.2021.105366.
[4] H. Hamzah, B. Sahin, Analysis of SWCNT-water nanofluid flow in wavy channel under turbulent pulsating conditions: investigation of homogeneous and discrete phase models, Int. J. Therm. Sci. 184 (2023), 108011, https://doi.org/10.1016/j.ijthermalsci.2022.108011.
[5] C.-C. Wang, C.-K. Chen, Forced convection in a wavy-wall channel, Int. J. Heat Mass Tran. 45 (2002) 2587–2595, https://doi.org/10.1016/s0017-9310(01)00335-0.
[6] A.M. Aly, A.J. Chamkha, S.-W. Lee, A. Al-Mudhaf, On mixed convection in an inclined lid-driven cavity with sinusoidal heated walls using the ISPH method, Comput. Therm. Sci.: Int. J. 8 (2016) 337–354, https://doi.org/10.1615/computthermalscien.2016016527.
[7] M.A. Ahmed, N.H. Shuaib, M.Z. Yusoff, A.H. Al-Falahi, Numerical investigations of flow and heat transfer enhancement in a corrugated channel using nanofluid, Int. Commun. Heat Mass Tran. 38 (2011) 1368–1375, https://doi.org/10.1016/j.icheatmasstransfer.2011.08.013.
[8] M.A. Ahmed, N.H. Shuaib, M.Z. Yusoff, Numerical investigations on the heat transfer enhancement in a wavy channel using nanofluid, Int. J. Heat Mass Tran. 55 (2012) 5891–5898, https://doi.org/10.1016/j.ijheatmasstransfer.2012.05.086.
[9] M.A. Ahmed, M.Z. Yusoff, N.H. Shuaib, Effects of geometrical parameters on the flow and heat transfer characteristics in trapezoidal-corrugated channel using nanofluid, Int. Commun. Heat Mass Tran. 42 (2013) 69–74, https://doi.org/10.1016/j.icheatmasstransfer.2012.12.012.
[10] A.A.R. Darzi, M. Farhadi, K. Sedighi, S. Aallahyari, M.A. Delavar, Turbulent heat transfer of Al_2O_3–water nanofluid inside helically corrugated tubes: numerical study, Int. Commun. Heat Mass Tran. 41 (2013) 68–75, https://doi.org/10.1016/j.icheatmasstransfer.2012.11.006.
[11] H.A. Mohammed, P. Gunnasegaran, N.H. Shuaib, Numerical simulation of heat transfer enhancement in wavy microchannel heat sink, Int. Commun. Heat Mass Tran. 38 (2011) 63–68, https://doi.org/10.1016/j.icheatmasstransfer.2010.09.012.
[12] N. Kurtulmuş, H. Zontul, B. Sahin, Heat transfer and flow characteristics in a sinusoidally curved converging-diverging channel, Int. J. Therm. Sci. 148 (2020), 106163, https://doi.org/10.1016/j.ijthermalsci.2019.106163.

[13] A.M. Aly, Z.A. Raizah, M. Sheikholeslami, Analysis of mixed convection in a sloshing porous cavity filled with a nanofluid using ISPH method, J. Therm. Anal. Calorim. 139 (2019) 1977–1991, https://doi.org/10.1007/s10973-019-08575-0.

[14] N. Biswas, P.S. Mahapatra, N.K. Manna, Mixed convection heat transfer in a grooved channel with injection, Numer. Heat Tran., Part A: Applications 68 (2015) 663–685, https://doi.org/10.1080/10407782.2014.994411.

[15] A.M. Aly, M. Asai, A.J. Chamkha, Analysis of unsteady mixed convection in lid-driven cavity included circular cylinders motion using an incompressible smoothed particle hydrodynamics method, Int. J. Numer. Methods Heat Fluid Flow 25 (2015) 2000–2021, https://doi.org/10.1108/hff-10-2014-0305.

[16] N. Biswas, N.K. Manna, Enhanced convective heat transfer in lid-driven porous cavity with aspiration, Int. J. Heat Mass Tran. 114 (2017) 430–452, https://doi.org/10.1016/j.ijheatmasstransfer.2017.06.078.

[17] N. Biswas, N. Kumar Manna, A. Mukhopadhyay, S. Sen, Numerical simulation of laminar confined radial flow between parallel circular discs, J. Fluid Eng. 134 (2012), https://doi.org/10.1115/1.4005737.

[18] A. Chakravarty, N. Biswas, K. Ghosh, N.K. Manna, A. Mukhopadhyay, S. Sen, Impact of side injection on heat removal from truncated conical heat-generating porous bed: thermal non-equilibrium approach, J. Therm. Anal. Calorim. 143 (2020) 3741–3760, https://doi.org/10.1007/s10973-020-09295-6.

[19] H. Hamzah, A. Albojamal, B. Sahin, K. Vafai, Thermal management of transverse magnetic source effects on nanofluid natural convection in a wavy porous enclosure, J. Therm. Anal. Calorim. 143 (2020) 2851–2865, https://doi.org/10.1007/s10973-020-10246-4.

[20] H. Zontul, H. Hamzah, B. Sahin, Impact of periodic magnetic source on natural convection and entropy generation of ferrofluids in a baffled cavity, Int. J. Numer. Methods Heat Fluid Flow 31 (2021) 3547–3575, https://doi.org/10.1108/hff-10-2020-0671.

[21] A. Asadi, A. Hossein Nezhad, F. Sarhaddi, T. Keykha, Laminar ferrofluid heat transfer in presence of non-uniform magnetic field in a channel with sinusoidal wall: a numerical study, J. Magn. Magn Mater. 471 (2019) 56–63, https://doi.org/10.1016/j.jmmm.2018.09.045.

[22] H. Heidary, M. Kermani, B. Dabir, Magnetic field effect on convective heat transfer in corrugated flow channel, Therm. Sci. 21 (2017) 2105–2115, https://doi.org/10.2298/tsci140610002h.

[23] H. Aminfar, M. Mohammadpourfard, S. Ahangar Zonouzi, Hydrothermal behavior of a ferrofluid in a corrugated channel in the presence of a magnetic field, Heat Tran. Asian Res. 43 (2013) 80–92, https://doi.org/10.1002/htj.21060.

[24] N. Biswas, A.J. Chamkha, N.K. Manna, Energy-saving method of heat transfer enhancement during magneto-thermal convection in typical thermal cavities adopting aspiration, SN Appl. Sci. 2 (2020), https://doi.org/10.1007/s42452-020-03634-w.

[25] S.E. Ahmed, M.A. Mansour, A.M. Alwatban, A.M. Aly, Finite element simulation for MHD ferro-convective flow in an inclined double-lid driven L-shaped enclosure with heated corners, Alex. Eng. J. 59 (2020) 217–226, https://doi.org/10.1016/j.aej.2019.12.026.

[26] S. Mei, C. Qi, T. Luo, X. Zhai, Y. Yan, Effects of magnetic field on thermo-hydraulic performance of FE3O4-water nanofluids in a corrugated tube, Int. J. Heat Mass Tran. 128 (2019) 24–45, https://doi.org/10.1016/j.ijheatmasstransfer.2018.08.071.

[27] M.M. Larimi, A. Ghanaat, A. Ramiar, A.A. Ranjbar, Forced convection heat transfer in a channel under the influence of various non-uniform transverse magnetic field arrangements, Int. J. Mech. Sci. 118 (2016) 101–112, https://doi.org/10.1016/j.ijmecsci.2016.09.023.

[28] M.M. Rashidi, M. Nasiri, M. Khezerloo, N. Laraqi, Numerical investigation of magnetic field effect on mixed convection heat transfer of nanofluid in a channel with sinusoidal walls, J. Magn. Magn Mater. 401 (2016) 159–168, https://doi.org/10.1016/j.jmmm.2015.10.034.

[29] M.M. Ali, R. Akhter, M.A. Alim, MHD natural convection and entropy generation in a grooved enclosure filled with nanofluid using two-component non-homogeneous model, SN Appl. Sci. 2 (2020), https://doi.org/10.1007/s42452-020-2319-x.

[30] H. Shaker, M. Abbasalizadeh, S. Khalilarya, S.Y. Motlagh, Two-phase modeling of the effect of non-uniform magnetic field on mixed convection of magnetic nanofluid inside an open cavity, Int. J. Mech. Sci. 207 (2021), 106666, https://doi.org/10.1016/j.ijmecsci.2021.106666.

[31] S.M. Mousavi, M. Biglarian, A.A. Darzi, M. Farhadi, H.H. Afrouzi, D. Toghraie, Heat transfer enhancement of ferrofluid flow within a wavy channel by applying a non-uniform magnetic field, J. Therm. Anal. Calorim. 139 (2019) 3331–3343, https://doi.org/10.1007/s10973-019-08650-6.

[32] D. Sáchica, C. Treviño, L. Martínez-Suástegui, Numerical study of magnetohydrodynamic mixed convection and entropy generation of Al_2O_3-water nanofluid in a channel with two facing cavities with discrete heating, Int. J. Heat Fluid Flow 86 (2020), 108713.

[33] Z. Mehrez, A. El Cafsi, A. Belghith, P. Le Quéré, MHD effects on heat transfer and entropy generation of nanofluid flow in an open cavity, J. Magn. Magn Mater. 374 (2015) 214–224, https://doi.org/10.1016/j.jmmm.2014.08.010.

[34] F. Selimefendigil, H.F. Öztop, Influence of inclination angle of magnetic field on mixed convection of nanofluid flow over a backward facing step and entropy generation, Adv. Powder Technol. 26 (2015) 1663–1675, https://doi.org/10.1016/j.apt.2015.10.002.

[35] A.M. Aly, ISPH method for MHD convective flow from grooves inside a nanofluid-filled cavity under the effects of Soret and Dufour numbers, Phys. Stat. Mech. Appl. 546 (2020), 124087, https://doi.org/10.1016/j.physa.2019.124087.

[36] N. Biswas, N.K. Manna, A. Datta, D.K. Mandal, A.C. Benim, Role of aspiration to enhance MHD convection in protruded heater cavity, Progress in Computational Fluid Dynamics, Int. J. 20 (2020) 363, https://doi.org/10.1504/pcfd.2020.111408.

[37] S. Dutta, S. Pati, L. Baranyi, Numerical Analysis of magnetohydrodynamic natural convection in a nanofluid filled quadrantal enclosure, Case Stud. Therm. Eng. 28 (2021), 101507, https://doi.org/10.1016/j.csite.2021.101507.

[38] S. Salehi, A. Nori, K. Hosseinzadeh, D.D. Ganji, Hydrothermal analysis of MHD squeezing mixture fluid suspended by hybrid nanoparticles between two parallel plates, Case Stud. Therm. Eng. 21 (2020), 100650, https://doi.org/10.1016/j.csite.2020.100650.

[39] C.-C. Liao, W.-K. Li, Assessment of the magnetic field influence on heat transfer transition of natural convection within a square cavity, Case Stud. Therm. Eng. 28 (2021), 101638, https://doi.org/10.1016/j.csite.2021.101638.

[40] N.B. Morley, S. Smolentsev, L. Barleon, I.R. Kirillov, M. Takahashi, Liquid magnetohydrodynamics — recent progress and future directions for fusion, Fusion Eng. Des. 51–52 (2000) 701–713, https://doi.org/10.1016/s0920-3796(00)00197-6.

[41] M. Sathiyamoorthy, A.J. Chamkha, Natural convection flow under magnetic field in a square cavity for uniformly (or) linearly heated adjacent walls, Int. J. Numer. Methods Heat Fluid Flow 22 (2012) 677–698, https://doi.org/10.1108/09615531211231307.

[42] F. Selimefendigil, H.F. Öztop, A.J. Chamkha, MHD mixed convection and entropy generation of nanofluid filled lid driven cavity under the influence of inclined magnetic fields imposed to its upper and lower diagonal triangular domains, J. Magn. Magn Mater. 406 (2016) 266–281, https://doi.org/10.1016/j.jmmm.2016.01.039.

[43] S. Tumse, H. Zontul, H. Hamzah, B. Sahin, Numerical investigation of magnetohydrodynamic forced convection and entropy production of ferrofluid around a confined cylinder using wire magnetic sources, Arabian J. Sci. Eng. (2022), https://doi.org/10.1007/s13369-022-07470-5.

[44] F. Garoosi, L. Jahanshaloo, M.M. Rashidi, A. Badakhsh, M.E. Ali, Numerical simulation of natural convection of the nanofluid in heat exchangers using a Buongiorno model, Appl. Math. Comput. 254 (2015) 183–203, https://doi.org/10.1016/j.amc.2014.12.116.

[45] F. Garoosi, G. Bagheri, F. Talebi, Numerical simulation of natural convection of nanofluids in a square cavity with several pairs of heaters and coolers (hacs) inside, Int. J. Heat Mass Tran. 67 (2013) 362–376, https://doi.org/10.1016/j.ijheatmasstransfer.2013.08.034.

[46] J. Buongiorno, Convective transport in nanofluids, J. Heat Tran. 128 (2005) 240–250, https://doi.org/10.1115/1.2150834.

[47] N. Biswas, N.K. Manna, P. Datta, P.S. Mahapatra, Analysis of heat transfer and pumping power for bottom-heated porous cavity saturated with Cu-water nanofluid, Powder Technol. 326 (2018) 356–369, https://doi.org/10.1016/j.powtec.2017.12.030.

[48] F. Garoosi, B. Rohani, M.M. Rashidi, Two-phase mixture modeling of mixed convection of nanofluids in a square cavity with internal and external heating, Powder Technol. 275 (2015) 304–321, https://doi.org/10.1016/j.powtec.2015.02.015.

[49] F. Garoosi, M.M. Rashidi, Conjugate-mixed convection heat transfer in a two-sided lid-driven cavity filled with nanofluid using Manninen's two phase model, Int. J. Mech. Sci. 131–132 (2017) 1026–1048, https://doi.org/10.1016/j.ijmecsci.2017.08.030.

[50] F.H. Ali, H.K. Hamzah, K. Egab, M. Arıcı, A. Shahsavar, Non-Newtonian nanofluid natural convection in a U-shaped cavity under magnetic field, Int. J. Mech. Sci. 186 (2020), 105887, https://doi.org/10.1016/j.ijmecsci.2020.105887.

[51] F. Selimefendigil, H.F. Öztop, Control of natural convection in a CNT-water nanofluid filled 3D cavity by using an inner T-shaped obstacle and thermoelectric cooler, Int. J. Mech. Sci. 169 (2020), 105104, https://doi.org/10.1016/j.ijmecsci.2019.105104.

[52] G.H.R. Kefayati, Simulation of heat transfer and entropy generation of MHD natural convection of non-Newtonian nanofluid in an enclosure, Int. J. Heat Mass Tran. 92 (2016) 1066–1089, https://doi.org/10.1016/j.ijheatmasstransfer.2015.09.078.
[53] M.A. Ahmed, M.Z. Yusoff, K.C. Ng, N.H. Shuaib, Effect of corrugation profile on the thermal–hydraulic performance of corrugated channels using cuo–water nanofluid, Case Stud. Therm. Eng. 4 (2014) 65–75, https://doi.org/10.1016/j.csite.2014.07.001.
[54] B. Ghasemi, S.M. Aminossadati, A. Raisi, Magnetic Field Effect on natural convection in a nanofluid-filled square enclosure, Int. J. Therm. Sci. 50 (2011) 1748–1756, https://doi.org/10.1016/j.ijthermalsci.2011.04.010.
[55] G.G. Ilis, M. Mobedi, B. Sunden, Effect of aspect ratio on entropy generation in a rectangular cavity with differentially heated vertical walls, Int. Commun. Heat Mass Tran. 35 (2008) 696–703, https://doi.org/10.1016/j.icheatmasstransfer.2008.02.002.